Environmental Pollution 367 (2025) 125602

Contents lists available at ScienceDirect

Environmental Pollution

journal homepage: www.elsevier.com/locate/envpol

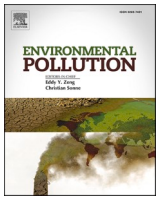

Application of a near real-time technique for the assessment of atmospheric arsenic and metals emissions from a copper smelter in an urban area of SW Europe☆

Pablo Pérez-Vizcaíno [a,b,*], Ana M. Sánchez de la Campa [a,b], Daniel Sánchez-Rodas [a,c], Jesús D. de la Rosa [a,b]

[a] Associate Unit CSIC-University of Huelva "Atmospheric Pollution", Center for Research in Sustainable Chemistry–CIQSO, University of Huelva, E21007, Huelva, Spain
[b] Department of Earth Sciences, Faculty of Experimental Sciences, University of Huelva, Campus El Carmen s/n, E21007, Huelva, Spain
[c] Department of Chemistry, Faculty of Experimental Sciences, University of Huelva, Campus El Carmen s/n, E21007, Huelva, Spain

ARTICLE INFO

Keywords:
Arsenic
Copper smelter
Near real-time
Hourly resolution
Saharan dust

ABSTRACT

Emissions of metals and metalloids as a result of industrial processes, entail a great risk to human health. A high time resolution study on arsenic levels in PM_{10} in the city of Huelva (SW Spain) was carried out between September 2021 and September 2022. Hourly data obtained with a near real-time technique based on X-ray fluorescence were inter-compared with other offline analytical instrumentation. The results showed that the main origin of As and other metal(loid)s such as Zn and Pb, was the copper smelter located southwest to the city. Although the mean concentration of As during the study period (2.8 ng m^{-3}) was lower than the target value (6 ng m^{-3}) proposed by the European Directive 2004/107/EC, hourly peaks of up to 311 ng m^{-3} were measured. The highest concentrations of arsenic were reached in the early afternoon, related to the influence of breeze. A source apportionment study has identified five major sources of PM_{10}: mineral, marine, combustion, regional and industry. The industrial source is characterized by high concentrations of As, Cu, Pb and Zn, contributing 1% of the total concentration of PM_{10} and related to copper smelter emissions. In addition, the analysis of two extreme North African dust outbreak events that affected southwestern Europe in March 2022, showed that this natural source contributed slightly to arsenic levels. The need to carry out high time resolution studies is demonstrated to better understand the variability in exposure to industrial metal(loid)s by the population, compared to conventional 24-h studies.

1. Introduction

Copper smelters (Cu-smelters) are one of the main anthropogenic sources of sulfur dioxide (SO_2) and sulfide-related elements in the atmosphere (e.g., Gidhagen et al., 2002; Carn et al., 2007; Serbula et al., 2014). The process of heating the ore to retrieve the blister copper causes the release of other elements into the air as dust. Metals and metalloids emitted in these industrial environments, such as arsenic (As), chromium (Cr), lead (Pb) and mercury (Hg) are among the most toxic pollutants threatening human health (McCartor and Becker, 2010), but others such as cadmium (Cd), nickel (Ni) and zinc (Zn) are also carcinogenic (Kim et al., 2015).

Arsenic exposure may not only affect and disable organs of the body, but may also interfere with the proper functioning of the immune system (Duker et al., 2005). Arsenic can cause cardiovascular (Lee et al., 2002) and respiratory (Milton and Rahman, 2002) diseases, diabetes and hypertension (Chen et al., 2007), hormonal and reproductive effects (Chakraborti et al., 2003), and skin, lung and urinary bladder cancer (e.g., Kapaj et al., 2006; Cantor and Lubin, 2007). In order to minimize its harmful effects on human health, the European Directive 2004/107/EC set a target value for atmospheric As concentrations in PM_{10} (particulate matter with aerodynamic diameter <10 μm) to be less than 6 ng m^{-3} averaged over a calendar year (European Commission, 2004). This target value has been repeatedly exceeded in the past in Huelva (de la

☆ This paper has been recommended for acceptance by Prof. Pavlos Kassomenos.

* Corresponding author. Associate Unit CSIC-University of Huelva "Atmospheric Pollution", Center for Research in Sustainable Chemistry–CIQSO, University of Huelva, E21071, Huelva, Spain.
E-mail address: pablo.perez@ciqso.uhu.es (P. Pérez-Vizcaíno).

https://doi.org/10.1016/j.envpol.2024.125602
Received 2 October 2024; Received in revised form 20 December 2024; Accepted 26 December 2024
Available online 27 December 2024

Fig. 1. Map of the study area: Campus monitoring station (red circle), Cu-smelter (yellow star), the three main industrial estates (I.E.) of the city (yellow shading) and wind rose diagram for the study period (Sep. 2021–Sep. 2022). (For interpretation of the references to colour in this figure legend, the reader is referred to the Web version of this article.)

Rosa et al., 2010; Sánchez de la Campa et al., 2011; Sánchez-Rodas et al., 2012), an area in SW Europe with a significant association between As, Cd, Cu, Pb and Zn, linked to industrial emissions, and mortality risk (Tobías et al., 2018). Several studies have been made with the aim of characterizing the air quality of the region (Querol et al., 2002; Alastuey et al., 2006; Sánchez de la Campa et al., 2007, 2018) and more specifically, the impact of As levels and related metals (e.g., Bi, Cu, Se, Zn) on the city of Huelva (Sánchez-Rodas et al., 2007; Fernández-Camacho et al., 2010; Chen et al., 2016; Millán-Martínez et al., 2021).

Previous studies in other areas with Cu-smelters (e.g., Gidhagen et al., 2002; Wong et al., 2006; Boyd et al., 2009; Kovačević et al., 2010; Sorooshian et al., 2012; Kim et al., 2016; Hu et al., 2019) have determined arsenic concentrations in PM_{10}. However, these works are based on 24-h offline sampling, thus omitting the hourly variations of As and any other element of interest. This causes the loss of information about its origin and correlation with other pollutants and meteorological parameters such as wind speed and direction. The use of near real-time (NRT) techniques (e.g., Xact 625i Ambient Metals Monitor) has been shown to be very useful for carrying out high time resolution studies for the measurement of As and other metal(loid)s. The Xact 625i has already been used in short field campaigns for quantification and source apportionment of PM in big cities (Park et al., 2014; Acciai et al., 2017; Manchanda et al., 2021; Shukla et al., 2021) or small towns (Belis et al., 2019), intercomparison with other spectrometry methods (Park et al.,

2014; Furger et al., 2017), evaluation of a firework episode (Rai et al., 2020) and identification of nickel sources in an industrial area (Font et al., 2022). Nevertheless, few long-term studies have been conducted by using this technique (Chang et al., 2018; Tremper et al., 2018; Yu et al., 2019; Hasheminassab et al., 2020; Manousakas et al., 2022).

This work presents a 12-month study (September 2021–September 2022) focused on the use of the NRT Xact 625i for the characterization of arsenic behavior in PM_{10} at a monitoring station located within the city of Huelva. We compared the results obtained with this high time resolution (1-h) instrument with those from chemical analysis of other low resolution (24-h) offline instrumentation, located at the same station, to validate them. Two extreme Saharan dust outbreak events that took place during the study period were also analyzed in detail with the aim of assessing if this natural source contributed significantly to arsenic levels.

2. Study area

The city of Huelva (ca. 143,000 inhabitants) is located in the SW of Spain and belongs to the autonomous region of Andalusia (Fig. 1). Huelva is over a flat area in the confluence of the Odiel and Tinto Rivers, thus defining the estuary known as the Ría of Huelva. This region has a transitional Mediterranean-Atlantic climate with mild winters and warm summers. The mean monthly maximum and minimum temperatures were 26.0 °C and 11.5 °C between 1991 and 2020, similar to the temperatures registered during the study period (mean monthly max. 26.8 °C, min. 10.9 °C). The total precipitation during the campaign was 203 mm. Information about wind direction and its temporal variation can be found in Sánchez de la Campa et al. (2007): the main directions are SW, NW and NE due to the Atlantic breeze (SW) and its circulation adapted to the estuarine topography (NW-Odiel and NE-Tinto Rivers valleys); the Atlantic component (W) predominates during January and is associated with low-pressure systems producing significant precipitation; February is characterized by NE and SW winds; in spring and summer, sea breeze regimes prevail, increasing wind speed during the afternoons with a SW component; N and NW are the main wind directions both November and December. In the study period, the prevailing wind directions came from the N and WSW (Fig. 1).

Huelva suffered an extensive industrialization process in the 1960s, when large chemical and petrochemical industries were set up. Nowadays, three industrial estates are recognized to the South of the city (Fig. 1): Punta del Sebo, Puerto Exterior and Nuevo Puerto. In the first, a phosphoric acid-based industry oriented to the production of phosphoric acid and phosphates, and a Cu-smelter plant are the most important industrial activities. This smelter has a production capacity of up to 320 kt per year (United States Geological Survey (USGS), 2003). In Puerto Exterior Industrial Estate, there is significant ship traffic, processes from petrochemical industry, and other activities (Millán-Martínez et al., 2021). A petrochemical industry (e.g., fuel oil, naphtha, gas oil and gasoline) and other activities such as TiO_2, chlorine and sodium hydroxide production are developed in Nuevo Puerto Industrial Estate. These industrial activities are more detailed in Querol et al. (2002). The wide variety of emission sources, the proximity of the industrial estates to the city and their coastal location favors the frequent impact of industrial emission plumes on Huelva. In addition, diurnal inland breeze often transports these plumes towards the city (Sánchez de la Campa et al., 2007).

The city is geographically located close to the North African coast, so it is affected by the frequent Saharan air masses coming from this region and crossing Europe. These dust outbreaks correspond to natural contributions of PM_{10} enriched in Al, Ca, Na, K, Mg and Fe, major constituents of the mineral material (mainly clay minerals) of North African soil (Sánchez de la Campa et al., 2007).

3. Methodology

3.1. $p.m._{10}$ and gaseous pollutants sampling

Between September 17th, 2021, to September 26th, 2022, continuous measurements of PM_{10} and gaseous pollutants (CO, NO, NO_2, NO_x, O_3 and SO_2) were carried out at the urban-industrial station of Campus (37°16′18"N, 6°55′31"W) by using automatic online instrumentation.

For PM_{10} measurements, a Thermo Fisher Scientific model 5014i based on the radiometric principle of beta attenuation, was employed. A Teledyne API model 300E based on infrared absorption, was used for CO. For NO, NO_2 and NO_x measurements, the Teledyne API model T200 based on the detection of chemiluminescence, was employed. For the determination of O_3 concentration, a Teledyne API model 400E based on ultraviolet radiation absorption, was used. Finally, for SO_2 measurements, the Thermo Fisher Scientific model 43i based on the principle of fluorescence, was employed.

3.2. Arsenic and other metal(loid)s NRT sampling and analysis

During the same period as PM_{10} and gaseous pollutants, hourly concentrations of Al, As, Ba, Bi, Br, Ca, Cd, Cl, Cr, Cu, Fe, K, Mn, Ni, Pb, Rb, S, Sb, Se, Si, Sn, Sr, Ti, V and Zn in PM_{10} were measured at Campus with the Cooper Environmental Services Xact 625i Ambient Metals Monitor located in a mobile unit next to the station.

This NRT instrument is based on reel-to-reel filter tape sampling followed by nondestructive X-ray fluorescence (XRF) analysis. In this campaign, Teflon filter tape was used and replaced every 20–25 days with a new one. Sampling time resolution was 1 h and ambient air particles were sampled with a flow rate of 16.69 L min^{-1} through the PM_{10} inlet. The PM deposit on the tape is excited with an X-ray tube in three energy conditions and a silicon drift detector measures the resulting XRF. During this analysis, a new sample is collected on the next clean spot of the filter tape located 2 inches away. NRT measurements are achieved by conducting continuous sampling and analysis simultaneously, except for the time required to advance the tape (~20 s) and the time required for daily automated quality assurance (QA) checks, performed every night at midnight (30 min). The electric current inside the mobile unit as well as the proper functioning of the instrument (e.g., X-ray tube temperature and sampling flow rate) were checked twice a day during the campaign.

3.3. Statistical analysis and receptor model

A correction factor (CF) was applied to Xact 625i hourly data after the inter-comparison carried out with offline analytical techniques: Ion Chromatography (IC) and Inductively Coupled Plasma – Optical Emission Spectrometry (ICP-OES) or – Mass Spectrometry (ICP-MS). This comparison showed an overestimation of Xact 625i measurements for As (CF = 0.90) and S (CF = 0.95). For the rest, the CFs were greater than 1, ranging from Cu (CF = 1.02) to Ni (CF = 3.02) (Supplementary Material, Table S1, and Fig. S1). However, some elements were not taken into account in the discussion of results because they had a weak correlation due to low concentrations, being close to the limit of detection (Ba, Cd, Sb, Se and Sn). To validate the corrected Xact 625i data, goodness-of-fit indicators were calculated without applying the CF and applying it (Table S2). With the application of CF, an improvement in the values of these indicators was obtained (Table S3), suggesting a moderate fit between Xact 625i and offline instrumentation. To assess the significance of the intercomparison, p-values (0.05) were also calculated for each element. The application of the CF displayed a good statistical significance (p-value >0.05) for most of them (Table S4).

Methodology of offline sampling and chemical analysis of elements in PM_{10} are described in Supplementary Material, including precision and accuracy of filter analysis per element. Hourly data processing of meteorological parameters, conventional pollutants and metal(loid)s

Table 1
Statistical parameters (ng m^{-3}) of elements measured at Campus monitoring station (17th Sept. 2021–26th Sept. 2022) with Xact 625i; Mean: arithmetic mean; Sd: standard deviation; Q25%, Q50%, Q75%: quartile 25%, 50%, 75%; IQR: inter-quartile range; Max: maximum; N: number of hourly observations >1/2 LOD; %: percentage of observations >1/2 LOD compared to the total hours of the campaign (8998 h). The LODs for Rb and Sr are not determined (ND).

Element	Mean	Sd	Q25%	Q50%	Q75%	IQR	Max	N	%
Al	524	1805	57.5	157	460	403	36637	5440	60.5
As	2.8	7.7	0.2	0.9	2.5	2.3	311	7411	82.4
Bi	0.4	3.8	0.2	0.2	0.2	0.0	328	482	5.4
Br	3.7	3.7	1.3	3.2	5.3	4.0	145	7692	85.5
Ca	1013	2159	190	506	1031	842	46410	7725	85.9
Cl	810	1264	63	302	1004	940	11153	7529	83.7
Cr	1.7	3.9	0.1	0.4	1.7	1.6	72.2	5355	59.5
Cu	16.1	48.0	1.1	4.1	11.0	9.9	1765	7484	83.2
Fe	539	1051	130	317	605	475	19075	7725	85.9
K	354	717	118	235	413	295	39347	7707	85.7
Mn	6.0	15.8	0.3	2.5	6.1	5.8	310	7034	78.2
Ni	1.3	2.7	0.2	0.2	1.2	1.1	48.2	3752	41.7
Pb	5.1	22.0	0.1	0.1	0.1	0.0	520	2124	23.6
Rb	1.3	3.1	0.3	0.6	1.2	0.9	48.6	ND	ND
S	386	398	137	282	525	388	8185	7706	85.6
Si	1565	4570	64.7	600	1579	1514	92471	7098	78.9
Sr	4.6	13.3	1.3	2.4	4.4	3.1	778	ND	ND
Ti	50.0	119	8.1	23.7	50.0	41.9	2234	7690	85.5
V	1.7	3.5	0.1	0.6	2.1	2.0	58.7	5815	64.6
Zn	18.6	35.4	3.8	9.1	19.8	16.0	951	7712	85.7

was carried out with the Openair package in R (Carslaw and Ropkins, 2012).

The goal of receptor models is to solve the chemical mass balance between measured species concentrations and sources profiles. In this study, the Positive Matrix Factorization model (PMF v5.0 EPA) was used as the method for estimating sources identification and contributions. The method is described in greater detail in Paatero and Tapper (1994) and Paatero (1997). PMF is a multivariate factor analysis tool that decomposes a matrix of speciated sample data (X) of i by j dimensions into two matrices: factor contributions (G) and factor profiles (F). The model is based on the following equation:

$$X_{ij} = \sum_{k-1}^{p} G_{ik} * F_{kj} + E_{ij} \quad \text{(eq. 1)}$$

where *i* is the number of samples and *j* the chemical species measured. The number of factors is expressed by *p*. G_{ik} is the contribution of each source to each sample, F_{kj} represents the concentration of the species from each source and E_{ij} is the residual for each sample/species.

PMF uses both sample concentration and user-provided uncertainty associated with the sample data to weight individual points. Results are obtained using the constraint that no sample can have significantly negative source contributions. The number of species selected in the PMF was chosen based on their signal-to-noise ratio (S/N) (Paatero and Hopke, 2003). Those elements with an S/N value > 2.2 were classified as "strong", those with 0.2 < S/N < 2.2 as "weak", and those with S/N < 0.2 as "bad". These last elements are not considered in the model. In our study, As, Bi, Br, Ca, Cl, Cu, Fe, K, Mn, S, Si and Zn were "strong", and Al, Cr, Ni, Pb, Rb, Sr and V were classified as "weak".

4. Results and discussion

4.1. Levels of PM_{10} and gaseous pollutants

The average concentration of PM_{10} in the study period was 22.9 μg m^{-3}, below the limit value of 40 μg m^{-3} during a calendar year established by the European Directive 2008/50/EC (European Commission, 2008). The daily limit value of 50 μg m^{-3} was exceeded 11 times, less than the 35 days set by the same directive. In the case of NO_2, the average concentration was 5.4 μg m^{-3}, lower than the limit value of 40 μg m^{-3} established by the Directive 2008/50/EC. The hourly limit value of 200 μg m^{-3} (not to be exceeded more than 18 times a calendar year) was not exceeded at any time. The average O_3 concentration was 57 μg m^{-3}. Finally, the average concentration of SO_2 was 3.4 μg m^{-3}. The hourly (350 μg m^{-3}, not more than 24 times) and daily (125 μg m^{-3}, not more than 3 times) limit values established by the Directive 2008/50/EC for SO_2, were not exceeded at any time. Nevertheless, the European Union (EU) proposed a new air quality directive in September 2022 that included, among other changes, halving the annual limits for PM_{10} and NO_2 (European Commission, 2024). This would not imply a problem for NO_2, but it would be for PM_{10} because the average concentration measured during this campaign would exceed the new EU annual limit (20 μg m^{-3}).

Information about temporal variation of these conventional pollutants can be found in Fig. S2. In the case of PM_{10}, the highest monthly average concentration was reached in March 2022 (42.4 μg m^{-3}), temporally correlated with two extreme North African dust events that affected mainland Spain (Rodríguez and López-Darias, 2024). For NO_2, two concentration peaks were observed throughout the day: 09:00 h and 21:00–22:00 h local time (LT). The Campus station is located close to the main avenue of the city and at the entrance of a highway, so the influence of the morning rush hours is very important. Its concentration values were clearly lower on weekends than on weekdays. The highest concentration was reached during winter months. O_3 reached its maximum values during the afternoon (15:00–17:00 h LT), coinciding with the minimum of NO_2, and its lowest values at 09:00 h LT, coinciding with the peak of NO_2. This is because NO_2 is one of the precursors of tropospheric ozone in urban environments (e.g., Sillman, 1999). The highest concentrations of O_3 were reached in summer, when the ozone-forming photochemical reactions develop more rapidly due to higher temperatures and solar radiation. The highest hourly values of SO_2 were reached around 15:00–16:00 h LT. Summer months were the ones with the highest concentrations, especially July 2022. In Fig. S3, their sources are identified with wind speed and direction data. The main sources of PM_{10} came from NE and SE, corresponding to the directions of arrival of North African air masses in SW Spain (Rodríguez et al., 2001). The origin of NO_2 was local, associated with traffic around the station. In the case of O_3, it came from more distal precursor sources. Finally, the origin of SO_2 was associated with the Cu-smelter of Punta del Sebo Industrial Estate, to the SW.

4.2. Hourly chemical composition of As and other metal(loid)s in PM_{10}

Arsenic had a mean concentration of 2.8 ng m^{-3} (Table 1), lower

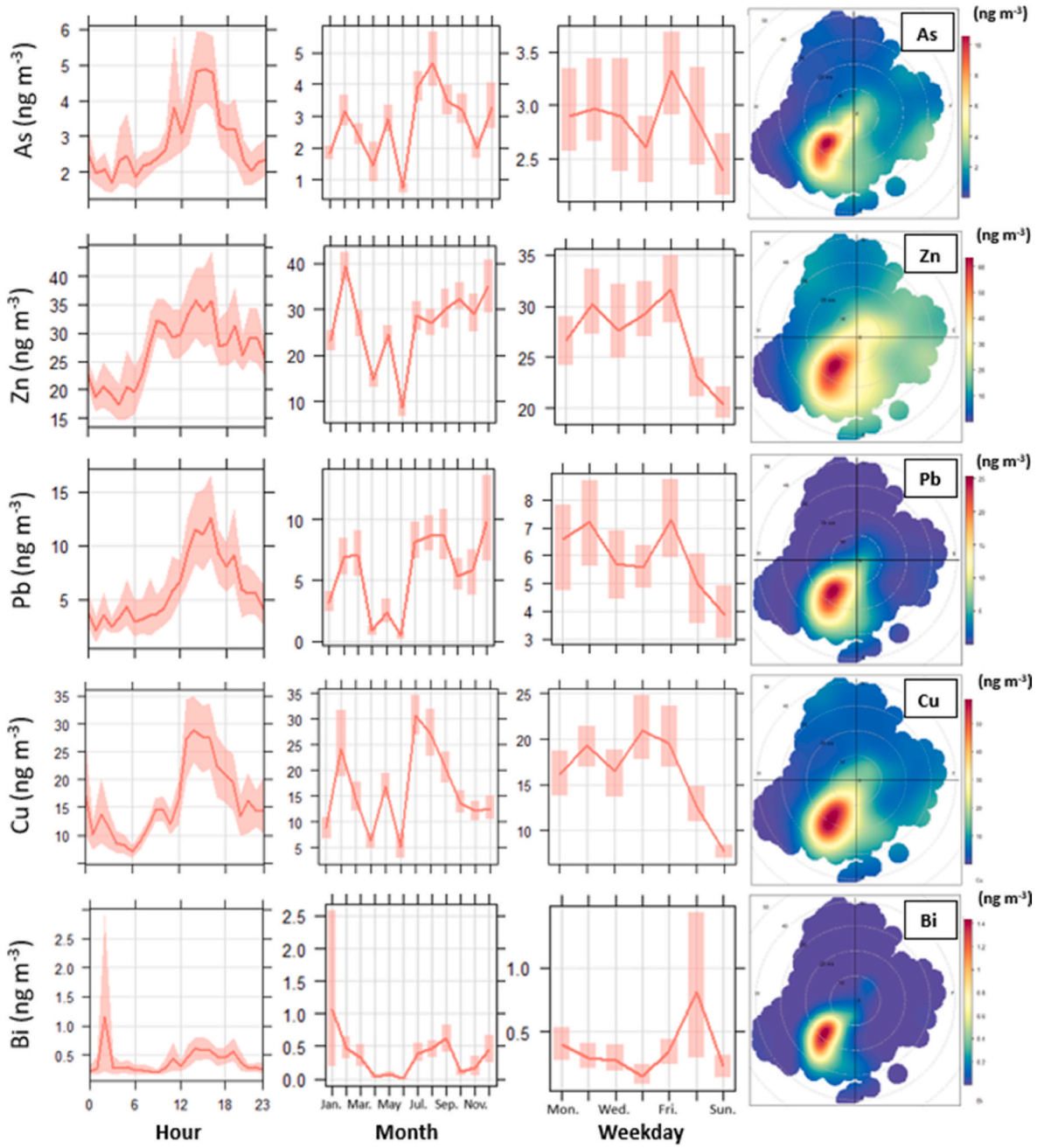

Fig. 2. Temporal variation and bivariate polar plots of industrial tracer elements (As, Zn, Pb, Cu and Bi) concentrations (ng m^{-3}) during the study period. Shaded area corresponds to the 95% confidence interval in mean.

than the target value (6 ng m^{-3}) set by the Directive 2004/107/EC. However, this value was exceeded 835 h, corresponding to 9.3% of the total for the study period. For the rest of the EU regulated heavy metals, the mean concentrations of Ni (1.3 ng m^{-3}) and Pb (5.1 ng m^{-3}) were also below the annual mean PM_{10} target values of 20 and 500 ng m^{-3}, respectively (European Commission, 2004; European Commission, 2008). The target value was exceeded 24 h (0.3%) for Ni and 1 h for Pb. The new EU directive will also involve the establishment of limit values for As, Cd, Ni and Pb (European Commission, 2024). Considering Al as a reference element, an enrichment factor (EF) greater than 40 was obtained for As and other associated metals (Table S5), showing a clear anthropogenic origin for these elements in relation to others with lower values (e.g., Fe, K and Rb) (Mummullage et al., 2016).

Arsenic concentrations in PM_{10} exhibited large variability during the campaign. The maximum hourly value was 311 ng m^{-3}. As showed a good correlation with other elements associated with polymetallic sulfides treated in the Cu-smelter of Punta del Sebo Industrial Estate such as Cu, Pb and Zn (Fig. S4). For As, Cu, Pb and Zn, the maximum mean values were measured in the early afternoon (14:00–16:00 h LT) due to the influence of the Atlantic breeze that allowed the arrival of industrial plumes from the smelter to the city (Fig. 2). On weekends, concentrations decreased in relation to weekdays, with Friday being the day with the highest values. The lowest mean concentrations were reached in June and the month with the highest values varied for each element: August, for As; July, for Cu; December, for Pb; February, for Zn. In the case of Bi, the bivariate polar plot was similar to that of As, Cu, Pb and Zn. The peak of concentration occurred during the early morning, although an increase in concentration was also identified in the early afternoon (Fig. 2). Saturday was the day with the highest mean values and January was the month with the highest concentration of Bi. June

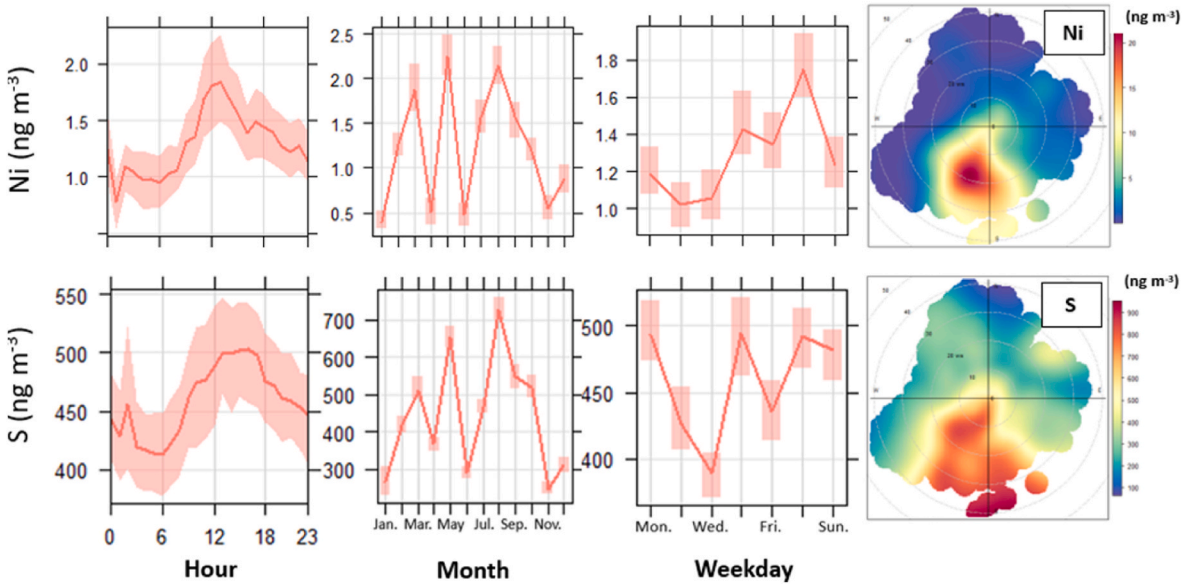

Fig. 3. Temporal variation and bivariate polar plots of industrial tracer elements (Ni and S) concentrations (ng m^{-3}) during the study period. Shaded area corresponds to the 95% confidence interval in mean.

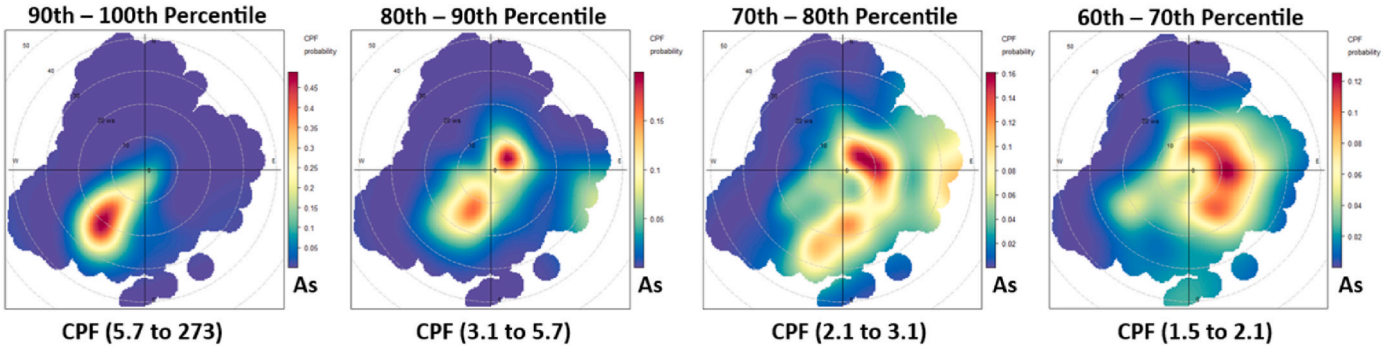

Fig. 4. Conditional bivariate probability function plots of As concentrations separated into four percentile ranges (90-100th, 80-90th, 70-80th and 60-70th).

was the month when the minimum concentrations were reached.

In the case of Ni and S, no correlation was observed with As (Fig. S4). The pattern of daily variation of Ni was similar to that of As, Cu, Pb and Zn, although in the case of Ni the concentration peak occurred a little earlier than the rest, around 13:00 h LT (Fig. 3). Saturday was the day with the highest mean concentration of Ni, similar to Bi, while for S high values were reached on Monday, Thursday and Saturday. Ni and S alternated months with high concentrations (March, May and August) and others with low concentrations (April, June and November). The origin of Ni seemed to correspond not only to the Cu-smelter, but also probably the petrochemical industry of Nuevo Puerto Industrial Estate, located to the South, and/or long-range transport from other combustion sources. In the case of S, its polar plot showed a mixture of the industrial activity carried out in the three industrial estates.

In this study, conditional bivariate probability function (CBPF) plots were applied to industrial tracer elements (Uria-Tellaetxe and Carslaw, 2014). These plots allow estimating the probability that a concentration value exceeds a set threshold taking into account wind speed and direction. A clear focus located in the opposite direction to the main source of the SW was identified for the range of 3.1–5.7 ng m^{-3} (Fig. 4). Considering the absence of arsenic-emitting sources to the NE of the city, this would correspond to the return of the Atlantic breeze still enriched with the plume of industrial elements from the Cu-smelter. At lower concentration ranges this focus was more diffuse, extending towards E and SE (Fig. 4). The return, which would not be possible to distinguish with 24-h sampling, was also observed in the CBPF plots of Cu, Pb and Zn, and not for Ni and S. This demonstrates a high residence time of As and other industrial elements, such as Zn and Pb, within the ultrafine particles range (Fernández-Camacho et al., 2012; González-Castanedo et al., 2014).

For the rest of the elements, the highest average hourly concentration was for Si with 1565 ng m^{-3} (Table 1). Ca was the second highest in concentration (1013 ng m^{-3}), followed by Cl (810 ng m^{-3}), Fe (539 ng m^{-3}), Al (524 ng m^{-3}), S (386 ng m^{-3}) and K (354 ng m^{-3}). The source of marine aerosol (Br and Cl) was distal and came from the S and SW (Fig. S5), where the Atlantic coast of Huelva is located. Both elements reached higher values on Saturdays, although their daily variation pattern was different: the maximum hourly mean value of Br at 15:00 h LT coincided approximately with the minimum of Cl. The main origin of crustal tracer elements (Rudnick and Gao, 2003) came from NE and SE (Fig. S6) because of the two extreme dust events during the campaign. In the case of Cr, a local source was also recognized. This source was attributed to traffic since this element is used as a friction material in brake pad manufacture (Amato et al., 2014). V showed two additional sources to the S and SW, related to the emissions from Punta del Sebo and Nuevo Puerto industrial estates. All crustal elements had an hourly peak of concentration around 09:00 h LT, because of the resuspension of particles during morning rush hours, and the maximum monthly mean value occurred in March 2022.

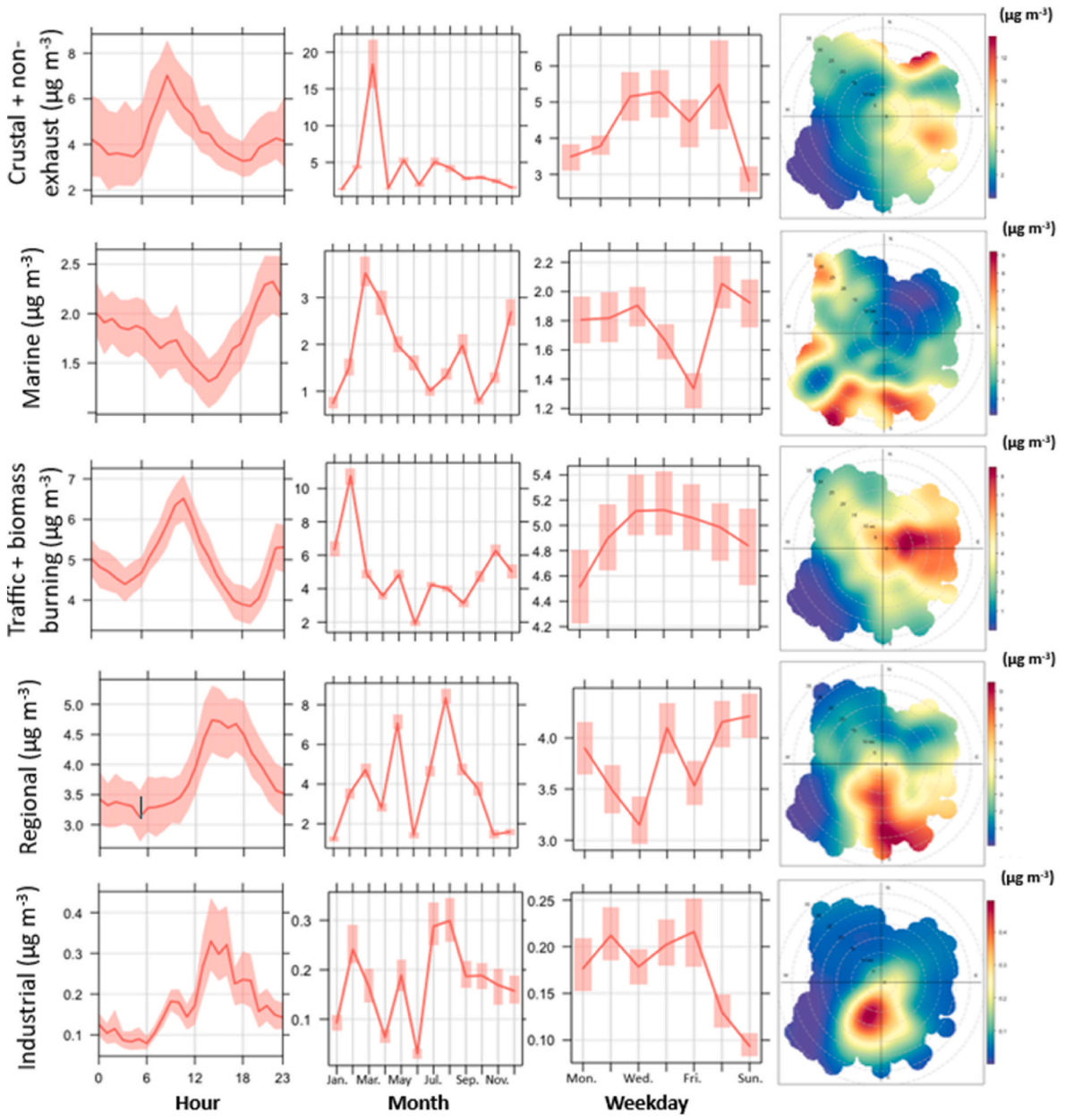

Fig. 5. Temporal variation and bivariate polar plots of source concentrations (µg m^{-3}) during the study period. Shaded area corresponds to the 95% confidence interval in mean.

4.3. Source apportionment

A PMF analysis was performed for Campus monitoring station in order to identify the natural and anthropogenic sources contributing to PM_{10} during the study period. The sources are similar to those obtained by Millán-Martínez et al. (2021) at the same station between 2015 and 2017 with offline instrumentation. A total of 5 sources were identified: mineral, marine, combustion, regional and industrial (Fig. 5 and Figs. S7–S8).

The first source is characterized by a mixture of crustal and non-exhaust trace elements (Al, Ca, Cr, Fe, K, Mn, Rb, Si, Sr, Ti and V). The main contribution factors to this source are the Saharan dust episodes and the local resuspension of particles during morning rush hours. This source contributes 29% to the total concentration of PM_{10}. The patterns of daily, weekly and annual variation are the same as those of crustal tracer elements (Fig. S6). The origin is located to the NE and SE due to the directions of arrival of North African air masses in SW Spain during the campaign.

A marine source, characterized by the typical sea salt components (mainly Cl and to a lesser extent, Br), was identified. The temporal variation is more similar to Cl than Br. The origin of this source is located to the SW, corresponding with the location of the Atlantic coast in Huelva. The contribution to the total PM_{10} was 12%.

The road traffic and biomass burning source is mainly characterized with exhaust emissions and K. This is the source that contributes the most to the concentration of PM_{10}, with 33%. The origin of the source is located to the E and NE. The daily variation pattern is characterized by a peak around 11:00 h LT and the lowest concentrations around 18:00–19:00 h LT.

A regional source characterized with Ni, S and V was identified, probably related to emissions of petrochemical activities and/or long-range transport. The patterns of daily, weekly and annual variation and the bivariate polar plot are more similar to S (Fig. 3) The contribution of this source is 25% and the origin is located to the S and SE,

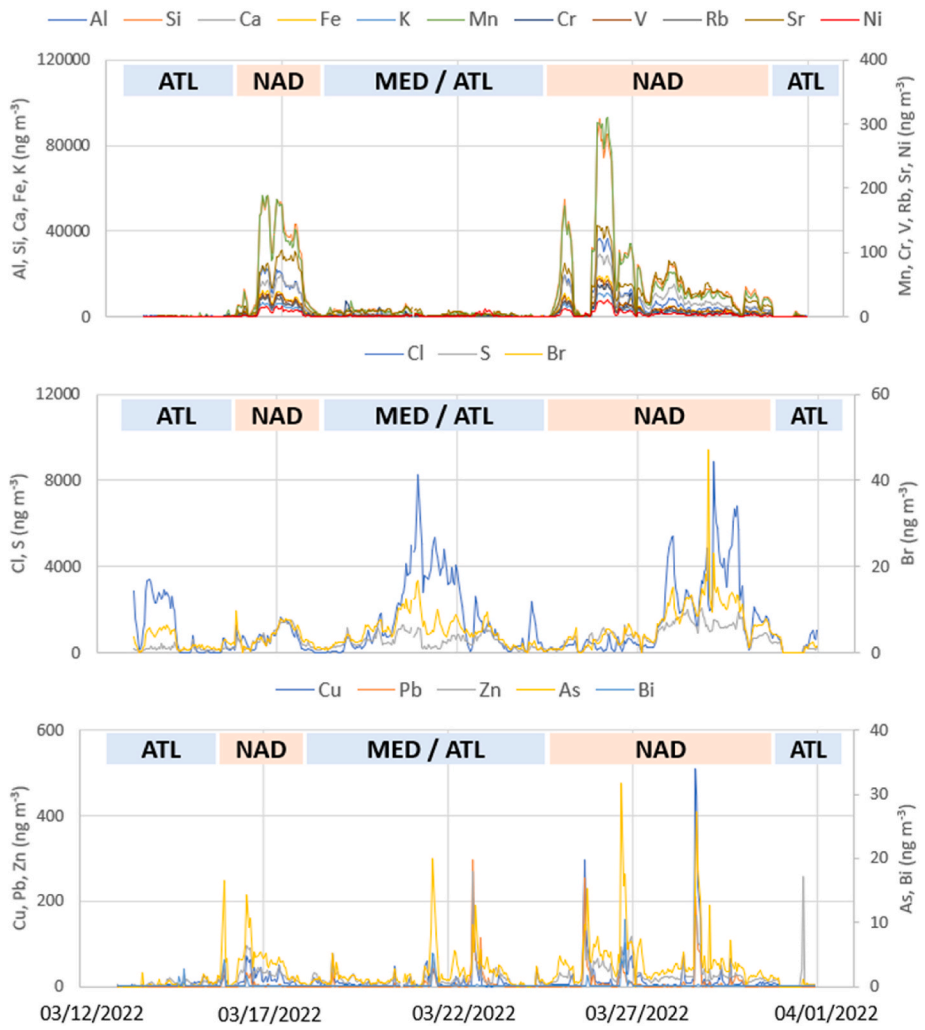

Fig. 6. Temporal variation diagram of elements analyzed with Xact 625i at Campus monitoring station between 13th-31st of March 2022. The origin of air masses has been indicated from their back trajectories: Atlantic (ATL), North African dust (NAD) and Mediterranean (MED).

corresponding with the location of Puerto Exterior and Nuevo Puerto industrial estates.

The industrial source only represents 1% to the total concentration of PM_{10} and is characterized by As, Cu, Pb and Zn. The patterns of daily and weekly variation are similar to those of these elements. This source has a clear origin to the SW, corresponding to the location of the Cu-smelter of Punta del Sebo Industrial Estate.

4.4. *Extreme North African dust events*

In the second half of March, the Iberian Peninsula was subjected to two episodes of intense Saharan air masses outbreaks, with Andalusia being one of the most affected regions of Spain. The first event took place between March 14th-17th and progressed from Eastern to Western Andalusia. It was linked to a low-pressure center located in North Africa and an anticyclonic core over the central Mediterranean (Rodríguez and López-Darias, 2024). The second event was temporally more prolonged and reached its maximum intensity between March 24th–27th. This episode was conditioned by another cyclone that evolved through North Africa, allowing the arrival of Saharan dust from East to West of Andalusia. In Huelva, the second episode was more intense, reaching its maximum on March 26th.

In the first event, the hourly mean value of the Ca/Al, Fe/Al and K/Al ratios were 1.01, 0.64 and 0.34, respectively. We have compared these values with those obtained at Izana Observatory (Tenerife, Spain) by Rodríguez et al. (2020) using hourly offline PIXE analysis. These authors describe 5 potential source areas (PSA) of dust masses in northern and central Africa according to their mineralogical composition. In the case of Ca/Al and K/Al ratios, the values measured at Campus station are more similar to those of PSA1 (~0.62 and up to 0.22, respectively), although they are higher. This PSA1 corresponds to northern Algeria. However, the mean value of the Fe/Al ratio at Campus is more similar to that of PSA3 (~0.49), corresponding to southern Algeria. The significant geographical distance between the areas of PSA1 and PSA3 suggest that the origin of the African air mass that took place in March 2022 was due to a mixing between both regions, close to the Hoggar massif (central Algeria). It should be taken into account that values of the ratios higher than those measured by Rodríguez et al. (2020) may also be influenced by the distance and enrichment in Ca, Fe and K before reaching Huelva and interferences from other sources during the transport of air masses. During the second event, the ratio values were even higher.

The pattern of temporal variation for crustal and non-exhaust trace elements (Al, Si, Ca, Fe, K, Mn, Cr, V, Rb and Sr) and Ni during the two huge dust outbreaks was similar (Fig. 6). For the first episode, a single peak of prolonged duration was registered and when it ended, the concentrations decreased sharply. Instead, higher but temporally shorter peaks were measured during the second episode and when it was over, concentrations decreased more progressively. Levels of marine aerosol (Br and Cl) were not as affected by the two North African air masses since their maximum values were not temporally correlated with

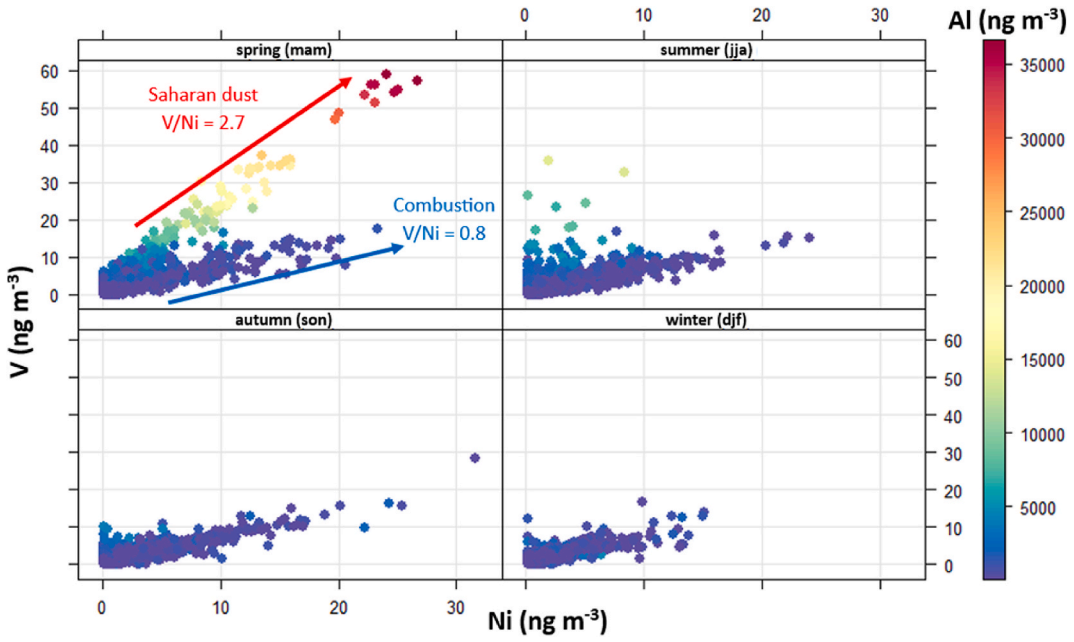

Fig. 7. Seasonal scatterplot of V vs Ni vs Al during the study period at Campus monitoring station. The two trends (Saharan dust and combustion) have been represented.

the days of high intensity of dust outbreaks (Fig. 5). The pattern of As, Bi, Cu, Pb and Zn was different from that of crustal elements and Ni, although punctual peaks were correlated with the two episodes (Fig. 6). This suggested that the extreme dust events were a very important source of Ni but of lesser importance for the rest of industrial tracer elements.

Bivariate polar plots of V and Ni and the evolution of their concentration during the two Saharan events, showed that the levels of these two elements were affected by natural and anthropic sources. In other studies (e.g., Moreno et al., 2010; Horemans et al., 2011; Zhao et al., 2013; Viana et al., 2014; Police et al., 2018), it has been observed that low values of the V/Ni ratio (~0.5) were associated with combustion processes. For most of the study period at Campus station, the trend of the V/Ni ratio value was 0.8 (Fig. 7), probably due to the influence of the industrial estates of Huelva. However, in spring an additional trend was recognized with a value of 2.7 (Fig. 7). The new trend was characterized by also high concentrations of crustal elements, such as Al. The value was within the typical range (V/Ni of 2–4) of North African dust episodes (Moreno et al., 2010). This suggests a relationship in which sources that cause an increase in Al concentration, would also imply an increase in the value of the V/Ni ratio.

5. Conclusions

In this 12-month high time resolution study, carried out at the urban-industrial station of Campus (Huelva, SW Europe), it has been found that metals and metalloids analyzed presented an important hourly variation. In some cases, with a maximum hourly value of up to two orders of magnitude higher than the mean value. In addition, its concentrations depended on meteorological factors such as the Atlantic breeze and its return. This causes a re-exposure in the population to metal(loid)s such as As, Cu, Pb and Zn due to their high residence time. It has also been possible to clearly identify the geographical position of the emission sources, corresponding in this case to the copper smelter located SW of the city. Finally, very high levels of crustal tracer elements were observed during two extreme North African dust outbreaks events, exceeding the daily limit value for PM_{10} (50 μg m^{-3}) considering only Ca, Si and Fe.

Similar to other conventional pollutants such as gases, PM_{10}, and $PM_{2.5}$, the present work highlights the need for high temporal resolution studies and continuous monitoring of As and metals in particulate matter in urban areas affected by industrial emissions, in order to control and minimize population exposure.

CRediT authorship contribution statement

Pablo Pérez-Vizcaíno: Writing – original draft, Investigation. **Ana M. Sánchez de la Campa:** Writing – review & editing, Methodology. **Daniel Sánchez-Rodas:** Writing – review & editing, Methodology. **Jesús D. de la Rosa:** Writing – review & editing, Funding acquisition.

Declaration of competing interest

The authors declare the following financial interests/personal relationships which may be considered as potential competing interests: Jesus Damian de la Rosa Diaz reports financial support was provided by Spain Ministry of Science and Innovation. Pablo Perez Vizcaino reports financial support was provided by Spain Ministry of Science and Innovation. Pablo Perez Vizcaino reports a relationship with Spain Ministry of Science and Innovation that includes: funding grants. If there are other authors, they declare that they have no known competing financial interests or personal relationships that could have appeared to influence the work reported in this paper.

Acknowledgments

This project has received funding from the European Union's Horizon 2020 research and innovation programme under grant agreement No 101036245. We would like to acknowledge the project of the Ministry of Science, Innovation, and Universities of Spain (Project RTI 2018-095937-B-I00 and PID2021-126986OB-I00) and the Environmental Agency of Andalusia for financial and technical support. Funding for open access charge: Universidad de Huelva/CBUA.

Appendix A. Supplementary data

Supplementary data to this article can be found online at https://doi.org/10.1016/j.envpol.2024.125602.

Data availability

Data will be made available on request.

References

Acciai, C., Zhang, Z., Wang, F., Zhong, Z., Lonati, G., 2017. Characteristics and source analysis of trace elements in $PM_{2.5}$ in the urban atmosphere of Wuhan in spring. Aerosol Air Qual. Res. 17, 2224–2234. https://doi.org/10.4209/aaqr.2017.06.0207.

Alastuey, A., Querol, X., Plana, F., Viana, M., Ruiz, C.R., Sánchez de la Campa, A., de la Rosa, J., Mantilla, E., García ds Santos, S., 2006. Identification and chemical characterization of industrial PM sources in SW Spain. J. Air Waste Manag. 56, 993–1006. https://doi.org/10.1080/10473289.2006.10464502.

Amato, F., Alastuey, A., de la Rosa, J., González Castanedo, Y., Sánchez de la Campa, A. M., Pandolfi, M., Lozano, A., Contreras González, J., Querol, X., 2014. Trends of road dust emissions contributions on ambient air particulate levels at rural, urban and industrial sites in southern Spain. Atmos. Chem. Phys. 14, 3533–3544. https://doi.org/10.5194/acp-14-3533-2014.

Belis, C.A., Pikridas, M., Lucarelli, F., Petralia, E., Cavalli, F., Calzolai, G., Berico, M., Sciare, J., 2019. Source apportionment of fine PM by combining high time resolution organic and inorganic chemical composition datasets. Atmos. Environ. X 3, 100046. https://doi.org/10.1016/j.aeaoa.2019.100046.

Boyd, R., Barnes, S.J., De Caritat, P., Chekushin, V.A., Melezhik, V.A., Reimann, C., Zientek, M.L., 2009. Emissions from the copper-nickel industry on the kola Peninsula and at Noril'sk, Russia. Atmos. Environ. 43, 1474–1480. https://doi.org/10.1016/j.atmosenv.2008.12.003.

Cantor, K.P., Lubin, J.H., 2007. Arsenic, internal cancers, and issues in inference from studies of low-level exposures in human populations. Toxicol. Appl. Pharmacol. 222, 252–257. https://doi.org/10.1016/j.taap.2007.01.026.

Carn, S.A., Krueger, A.J., Krotchov, N.A., Yang, K., Levelt, P.F., 2007. Sulfur dioxide emissions from Peruvian copper smelters detected by the Ozone Monitoring Instrument. Geophys. Res. Lett. 34, L09081. https://doi.org/10.1029/2006GL029020.

Carslaw, D.C., Ropkins, K., 2012. *Openair* – an R package for air quality data analysis. Environ. Model. Software 27–28, 52–61. https://doi.org/10.1016/j.envsoft.2011.09.008.

Chakraborti, D., Mukherjee, S.C., Pati, S., Sengupta, M.K., Rahman, M.M., Chowdhury, U.K., Lodh, D., Chanda, C.R., Chakraborti, A.K., Basu, G.K., 2003. Arsenic groundwater contamination in Middle Ganga Plain, Bihar, India: a future danger? Environ. Health Perspect. 111, 1194–1201. https://doi.org/10.1289/ehp.5966.

Chang, Y., Huang, K., Xie, M., Deng, C., Zou, Z., Liu, S., Zhang, Y., 2018. First long-term and near real-time measurement of trace elements in China's urban atmosphere: temporal variability, source apportionment and precipitation effect. Atmos. Chem. Phys. 18, 11793–11812. https://doi.org/10.5194/acp-18-11793-2018.

Chen, B., Stein, A.F., Castell, N., González-Castanedo, Y., Sánchez de la Campa, A.M., de la Rosa, J.D., 2016. Modeling and evaluation of urban pollution events of atmospheric heavy metals from a large Cu-smelter. Sci. Total Environ. 539, 17–25. https://doi.org/10.1016/j.scitotenv.2015.08.117.

Chen, C.-J., Wang, S.-L., Chiou, J.-M., Tseng, C.-H., Chiou, H.-Y., Hsueh, Y.-M., Chen, S.-Y., Wu, M.-M., Lai, M.-S., 2007. Arsenic and diabetes and hypertension in human populations: a review. Toxicol. Appl. Pharmacol. 222, 298–304. https://doi.org/10.1016/j.taap.2006.12.032.

De la Rosa, J.D., Sánchez de la Campa, A.M., Alastuey, A., Querol, X., González-Castanedo, Y., Fernández-Camacho, R., Stein, A.F., 2010. Using PM_{10} geochemical maps for defining the origin of atmospheric pollution in Andalusia (Southern Spain). Atmos. Environ. 44, 4595–4605. https://doi.org/10.1016/j.atmosenv.2010.08.009.

Duker, A.A., Carranza, E.J.M., Hale, M., 2005. Arsenic geochemistry and health. Environ. Int. 31, 631–641. https://doi.org/10.1016/j.envint.2004.10.020.

European Commission, 2004. Directive 2004/107/EC of the European Parliament and of the Council of 15/12/2004 relating to arsenic, cadmium, mercury, nickel and polycyclic aromatic hydrocarbons in ambient air. https://n9.cl/k7uo4 (accessed September 2024).

European Commission, 2008. Directive 2008/50/EC of the European Parliament and of the Council of 21/05/2008 on ambient air quality and cleaner air for Europe. https://n9.cl/ecxs2f (accessed September 2024).

European Commission, 2024. Directive 2024/2881/EC of the European Parliament and of the Council of 23/10/2024 on ambient air quality and cleaner air for Europe. https://n9.cl/9vums (accessed November 2024).

Fernández-Camacho, R., de la Rosa, J., Sánchez de la Campa, A.M., González-Castanedo, Y., Alastuey, A., Querol, X., Rodríguez, S., 2010. Atmos. Res. 96, 590–601. https://doi.org/10.1016/j.atmosres.2010.01.008.

Fernández-Camacho, R., Rodríguez, S., de la Rosa, J., Sánchez de la Campa, A.M., Alastuey, A., Querol, X., González-Castanedo, Y., García-Orellana, I., Nava, S., 2012. Ultrafine particle and fine trace metal (As, Cd, Cu, Pb and Zn) pollution episodes induced by industrial emissions in Huelva, SW Spain. Atmos. Environ. 61, 507–517. https://doi.org/10.1016/j.atmosenv.2012.08.003.

Font, A., Tremper, A.H., Priestman, M., Kelly, F.J., Canonaco, F., Prévot, A.S.H., Green, D.C., 2022. Source attribution and quantification of atmospheric nickel concentrations in an industrial area in the United Kingdom (UK). Environ. Pollut. 293, 118432. https://doi.org/10.1016/j.envpol.2021.118432.

Furger, M., Minguillón, M.C., Yadav, V., Slowik, J.G., Hüglin, C., Fröhlich, R., Petterson, K., Baltensperger, U., Prévot, A.S.H., 2017. Elemental composition of ambient aerosols measured with high temporal resolution using an online XRF spectrometer. Atmos. Meas. Tech. 10, 2061–2076. https://doi.org/10.5194/amt-10-2061-2017.

Gidhagen, L., Kahelin, H., Schmidt-Thomé, P., Johansson, C., 2002. Anthropogenic and natural levels of arsenic in PM_{10} in Central and Northern Chile. Atmos. Environ. 36, 3803–3817. https://doi.org/10.1016/S1352-2310(02)00284-4.

González-Castanedo, Y., Moreno, T., Fernández-Camacho, R., Sánchez de la Campa, A. M., Alastuey, A., Querol, X., de la Rosa, J., 2014. Size distribution and chemical composition of particulate matter stack emissions in and around a copper smelter. Atmos. Environ. 98, 271–282. https://doi.org/10.1016/j.atmosenv.2014.08.057.

Hasheminassab, S., Sowlat, M.H., Pakbin, P., Katzenstein, A., Low, J., Polidori, A., 2020. High-time resolution and time-integrated measurements of particulate metals and elements in an environmental justice community within Los Angeles basin: spatio-temporal trends and source apportionment. Atmos. Environ. X 7, 100089. https://doi.org/10.1016/j.aeaoa.2020.100089.

Horemans, B., Cardell, C., Bencs, L., Kontozova-Deutsch, V., De Wael, K., Van Grieken, R., 2011. Evaluation of airborne particles at the Alhambra monument in Granada, Spain. Microchem. J. 99, 429–438. https://doi.org/10.1016/j.microc.2011.06.018.

Hu, Y., Zhou, J., Du, B., Liu, H., Zhang, W., Liang, J., Zhang, W., You, L., Zhou, J., 2019. Health risks to local residents from the exposure of heavy metals around the largest copper smelter in China. Ecotoxicol. Environ. Saf. 171, 329–336. https://doi.org/10.1016/j.ecoenv.2018.12.073.

Kapaj, S., Peterson, H., Liber, K., Bhattacharya, P., 2006. Human health effects from chronic arsenic poisoning-A review. J. Environ. Sci. Health 41, 2399–2428. https://doi.org/10.1080/10934520600873571.

Kim, H.S., Kim, Y.J., Seo, Y.R., 2015. An overview of carcinogenic heavy metal: molecular toxicity mechanism and prevention. J. Cancer Prevent. 20, 232–240. https://doi.org/10.15430/JCP.2015.20.4.232.

Kim, Y.D., Eom, S.Y., Yim, D.H., Kim, I.S., Won, H.K., Park, C.H., Kim, G.B., Yu, S.D., Choi, B.Y., Park, J.D., Kim, H., 2016. Environmental exposure to arsenic, lead and cadmium in people living near Janghang copper smelter in Korea. J. Kor. Med. Sci. 31, 489–496. https://doi.org/10.3346/jkms.2016.31.4.489.

Kovačević, R., Jovašević-Stojanović, M., Tasić, V., Milošević, N., Petrović, N., Stanković, S., Matić-Besarabić, S., 2010. Preliminary analysis of levels of arsenic and other metallic elements in PM_{10} sampled near copper smelter Bor (Serbia). Chem. Ind. Chem. Eng. Q. 16, 269–279. https://doi.org/10.2298/CICEQ091225049K.

Lee, M.-Y., Bae, O.-N., Chung, S.-M., Kang, K.-T., Lee, J.-Y., Chung, J.-H., 2002. Enhancement of platelet aggregation and thrombus formation by arsenic in drinking water: a contributing factor to cardiovascular disease. Toxicol. Appl. Pharmacol. 179, 83–88. https://doi.org/10.1006/taap.2001.9356.

Manchanda, C., Kumar, M., Singh, V., Faisal, M., Hazarika, N., Shukla, A., Lalchandani, V., Goel, V., Thamban, N., Ganguly, D., Tripathi, S.N., 2021. Variation in chemical composition and sources of $PM_{2.5}$ during the COVID-19 lockdown in Delhi. Environ. Int. 153, 106541. https://doi.org/10.1016/j.envint.2021.106541.

Manousakas, M., Furger, M., Daellenbach, K.R., Canonaco, F., Chen, G., Tobler, A., Rai, P., Qi, L., Tremper, A.H., Green, D., Hueglin, C., Slowik, J.G., El Haddad, I., Prevot, A.S.H., 2022. Source identification of the elemental fraction of particulate matter using size segregated, highly time-resolved data and an optimized source apportionment approach. Atmos. Environ. X 14, 100165. https://doi.org/10.1016/j.aeaoa.2022.100165.

McCartor, A., Becker, D., 2010. Top Six Toxic Threats, World's Worst Pollution Problems Report 2010. Blacksmith Institute, New York.

Millán-Martínez, M., Sánchez-Rodas, D., Sánchez de la Campa, A.M., Alastuey, A., Querol, X., de la Rosa, J.D., 2021. Source contribution and origin of PM10 and arsenic in a complex industrial region (Huelva, SW Spain). Environ. Pollut. 274, 116268. https://doi.org/10.1016/j.envpol.2020.116268.

Milton, A.H., Rahman, M., 2002. Respiratory effects and arsenic contaminated well water in Bangladesh. Int. J. Environ. Health Res. 12, 175–179. https://doi.org/10.1080/09603120220129346.

Moreno, T., Querol, X., Alastuey, A., de la Rosa, J., Sánchez de la Campa, A.M., Minguillón, M., Pandolfi, M., González-Castanedo, Y., Monfort, E., Gibbons, W., 2010. Variations in vanadium, nickel and lanthanoid element concentrations in urban air. Sci. Total Environ. 408, 4569–4579. https://doi.org/10.1016/j.scitotenv.2010.06.016.

Mummullage, S., Egodawatta, P., Ayoko, G.A., Goonetilleke, A., 2016. Use of physicochemical signatures to assess the sources of metals in urban road dust. Sci. Total Environ. 541, 1303–1309. https://doi.org/10.1016/j.scitotenv.2015.10.032.

Paatero, P., Tapper, U., 1994. Positive matrix factorization: a nonnegative factor model with optimal utilization of error estimates of data values. Environmetrics 5, 111–126. https://doi.org/10.1002/env.3170050203.

Paatero, P., 1997. Least square formulation of robust non-negative factor analysis. Chemometr. Intell. Lab. Syst. 3, 23–35. https://doi.org/10.1016/S0169-7439(96)00044-5.

Paatero, P., Hopke, P.K., 2003. Discarding or downweighting high-noise variables in factor analytic models. Anal. Chim. Acta 490, 277–289. https://doi.org/10.1016/S0003-2670(02)01643-4.

Park, S.-S., Cho, S.-Y., Jo, M.-R., Gong, B.-J., Park, J.-S., Lee, S.-J., 2014. Field evaluation of a near-real time elemental monitor and identification of element sources observed at an air monitoring supersite in Korea. Atmos. Pollut. Res. 5, 119–128. https://doi.org/10.5094/APR.2014.015.

Police, S., Sahu, S.K., Tiwari, M., Pandit, G.G., 2018. Chemical composition and source apportionment of $PM_{2.5}$ and $PM_{2.5\text{-}10}$ in Trombay (Mumbai, India), a coastal industrial area. Particuology 37, 143–153. https://doi.org/10.1016/j.partic.2017.09.006.

Querol, X., Alastuey, A., de la Rosa, J., Sánchez de la Campa, A., Plana, F., Ruiz, C.R., 2002. Source apportionment analysis of atmospheric particulates in an industrialized

urban site in southwestern Spain. Atmos. Environ. 36, 3113–3125. https://doi.org/10.1016/S1352-2310(02)00257-1.

Rai, P., Furger, M., Slowik, J.G., Canonaco, F., Fröhlich, R., Hüglin, C., Minguillón, M.C., Petterson, K., Baltensperger, U., Prévot, A.S.H., 2020. Source apportionment of highly time-resolved elements during a firework episode from a rural freeway site in Switzerland. Atmos. Chem. Phys. 20, 1657–1674. https://doi.org/10.5194/acp-20-1657-2020.

Rodríguez, S., Querol, X., Alastuey, A., Kallos, G., Kakaliagou, O., 2001. Saharan dust contributions to PM10 and TSP levels in Southern and Eastern Spain. Atmos. Environ. 35, 2433–2447. https://doi.org/10.1016/S1352-2310(00)00496-9.

Rodríguez, S., Calzolai, G., Chiari, M., Nava, S., García, M.I., López-Solano, J., Marrero, C., López-Darias, J., Cuevas, E., Alonso-Pérez, S., Prats, N., Amato, F., Lucarelli, F., Querol, X., 2020. Rapid changes of dust geochemistry in the Saharan Air Layer linked to sources and meteorology. Atmos. Environ. 223, 117186. https://doi.org/10.1016/j.atmosenv.2019.117186.

Rodríguez, S., López-Darias, J., 2024. Emerging extreme Saharan-dust events expand northward over the Atlantic and Europe prompting record-breaking PM_{10} and $PM_{2.5}$ episodes. EGUsphere 2024, 1–35. https://doi.org/10.5194/egusphere-2023-3083.

Rudnick, R.L., Gao, S., 2003. The composition of the continental crust. In: Holland, H.D., Turekian, K.K. (Eds.), Treatise on Chemistry, vol. 3. Elsevier-Pergamon, Oxford, pp. 1–64. https://doi.org/10.1016/b0-08-043751-6/03016-4. The Crust.

Sánchez de la Campa, A.M., de la Rosa, J., Querol, X., Alastuey, A., Mantilla, E., 2007. Geochemistry and origin of PM_{10} in the Huelva region, southwestern Spain. Environ. Res. 103, 305–316. https://doi.org/10.1016/j.envres.2006.06.011.

Sánchez de la Campa, A.M., de la Rosa, J., González-Castanedo, Y., Fernández-Camacho, R., Alastuey, A., Querol, X., Stein, A.F., Ramos, J.L., Rodríguez, S., García Orellana, I., Nava, S., 2011. Levels and chemical composition of PM in a city near a large Cu-smelter in Spain. J. Environ. Monit. 13, 1276. https://doi.org/10.1039/C0EM00708K.

Sánchez de la Campa, A.M., Sánchez-Rodas, D., Alsioufi, L., Alastuey, A., Querol, X., de la Rosa, J.D., 2018. Air quality trends in an industrialized area of SW Spain. J. Clean. Prod. 186, 465–474. https://doi.org/10.1016/j.jclepro.2018.03.122.

Sánchez-Rodas, D., Sánchez de la Campa, A.M., de la Rosa, J.D., Oliveira, V., Gómez Ariza, J.L., Querol, X., Alastuey, A., 2007. Arsenic speciation of atmospheric particulate matter (PM_{10}) in an industrialized urban site in southwestern Spain. Chemosphere 66, 1485–1493. https://doi.org/10.1016/j.chemosphere.2006.08.043.

Sánchez-Rodas, D., Sánchez de la Campa, A.M., Oliveira, V., de la Rosa, J., 2012. Health implications of the distribution of arsenic species in airborne particulate matter. J. Inorg. Biochem. 108, 112–114. https://doi.org/10.1016/j.jinorgbio.2011.11.023.

Serbula, S.M., Ilic, A.A., Kalinovic, J.V., Kalinovic, T.S., Petrovic, N.B., 2014. Assessment of air pollution originating from copper smelter in Bor (Serbia). Environ. Earth Sci. 71, 1651–1661. https://doi.org/10.1007/s12665-013-2569-7.

Shukla, A.K., Lalchandani, V., Bhattu, D., Dave, J.S., Rai, P., Thamban, N.M., Mishra, S., Gaddamidi, S., Tripathi, N., Vats, P., Rastogi, N., Sahu, L., Ganguly, D., Kumar, M., Singh, V., Gargava, P., Tripathi, S.N., 2021. Real-time quantification and source apportionment of fine particulate matter including organics and elements in Delhi during summertime. Atmos. Environ. 261, 118598. https://doi.org/10.1016/j.atmosenv.2021.118598.

Sillman, S., 1999. The relation between ozone, NO_x and hydrocarbons in urban and polluted rural environments. Atmos. Environ. 33, 1821–1845. https://doi.org/10.1016/S1352-2310(98)00345-8.

Sorooshian, A., Csavina, J., Shingler, T., Dey, S., Brechtel, F.J., Sáez, A.E., Betterton, E.A., 2012. Hygroscopic and chemical properties of aerosols collected near a copper smelter: implications for public and environmental health. Environ. Sci. Technol. 46, 9473–9480. https://doi.org/10.1021/es302275k.

Tobías, A., Rivas, I., Reche, C., Alastuey, A., Rodríguez, S., Fernández-Camacho, R., Sánchez de la Campa, A.M., de la Rosa, J., Sunyer, J., Querol, X., 2018. Short-term effects of ultrafine particles on daily mortality by primary vehicle exhaust versus secondary origin in three Spanish cities. Environ. Int. 111, 144–151. https://doi.org/10.1016/j.envint.2017.11.015.

Tremper, A.H., Font, A., Priestman, M., Hamad, S.H., Chung, T.S., Pribadi, A., Brown, R. J.C., Goddard, S.L., Grassineau, N., Petterson, K., Kelly, F.J., Green, D.C., 2018. Field and laboratory evaluation of a high time resolution x-ray fluorescence instrument for determining the elemental composition of ambient aerosols. Atmos. Meas. Tech. 11, 3541–3557. https://doi.org/10.5194/amt-11-3541-2018.

United States Geological Survey (USGS), 2003 accessed December 2024. pubs.usgs.gov/of/2003/of03-075/CSTable.txt.

Uria-Tellaetxe, I., Carslaw, D.C., 2014. Conditional bivariate probability function for source identification. Environ. Model. Software 59, 1–9. https://doi.org/10.1016/j.envsoft.2014.05.002.

Viana, M., Hammingh, P., Colette, A., Querol, X., Degraeuwe, B., de Vlieger, I., van Aardenne, J., 2014. Impact of maritime transport emissions on coastal air quality in Europe. Atmos. Environ. 90, 96–105. https://doi.org/10.1016/j.atmosenv.2014.03.046.

Wong, H.K.T., Banic, C.M., Robert, S., Nejedly, Z., Campbell, J.L., 2006. In-stack and in-plume characterization of particulate metals emitted from a copper smelter. Geochem. Explor. Environ. Anal. 6, 131–137. https://doi.org/10.1144/1467-7873/05-083.

Yu, Y., He, S., Wu, X., Zhang, C., Yao, Y., Liao, H., Wang, Q., Xie, M., 2019. $PM_{2.5}$ elements at an urban site in Yangtze River Delta, China: high time-resolved measurement and the application in source apportionment. Environ. Pollut. 253, 1089–1099. https://doi.org/10.1016/j.envpol.2019.07.096.

Zhao, M., Zhang, Y., Ma, W., Fu, Q., Yang, X., Li, C., Zhou, B., Yu, Q., Chen, L., 2013. Characteristics and ship traffic source identification of air pollutants in China's largest port. Atmos. Environ. 64, 277–286. https://doi.org/10.1016/j.atmosenv.2012.10.007.